nature materials

LETTERS

PUBLISHED ONLINE: 11 APRIL 2016 | DOI: 10.1038/NMAT4623

Tailoring the nature and strength of electron–phonon interactions in the $SrTiO_3$(001) 2D electron liquid

Z. Wang[1,2*], S. McKeown Walker[2], A. Tamai[2], Y. Wang[3,4], Z. Ristic[5], F. Y. Bruno[2], A. de la Torre[2], S. Riccò[2], N. C. Plumb[1], M. Shi[1], P. Hlawenka[6], J. Sánchez-Barriga[6], A. Varykhalov[6], T. K. Kim[7], M. Hoesch[7], P. D. C. King[8], W. Meevasana[9], U. Diebold[10], J. Mesot[1,5,11], B. Moritz[3], T. P. Devereaux[3,12], M. Radovic[1,13] and F. Baumberger[1,2,8*]

Surfaces and interfaces offer new possibilities for tailoring the many-body interactions that dominate the electrical and thermal properties of transition metal oxides[1–4]. Here, we use the prototypical two-dimensional electron liquid (2DEL) at the $SrTiO_3$(001) surface[5–7] to reveal a remarkably complex evolution of electron–phonon coupling with the tunable carrier density of this system. At low density, where superconductivity is found in the analogous 2DEL at the $LaAlO_3/SrTiO_3$ interface[8–13], our angle-resolved photoemission data show replica bands separated by 100 meV from the main bands. This is a hallmark of a coherent polaronic liquid and implies long-range coupling to a single longitudinal optical phonon branch. In the overdoped regime the preferential coupling to this branch decreases and the 2DEL undergoes a crossover to a more conventional metallic state with weaker short-range electron–phonon interaction. These results place constraints on the theoretical description of superconductivity and allow a unified understanding of the transport properties in $SrTiO_3$-based 2DELs.

Carrier concentration is a key parameter defining the ground state of correlated electron systems. At the $LaAlO_3/SrTiO_3$ interface, the 2DEL density can be tailored by field-effect gating. As the system is depleted of carriers, its ground state evolves from a high-mobility 2DEL[4] into a two-dimensional superconductor[8–10] with pseudogap behaviour[11] and possible pairing above T_c (ref. 12). An analogous 2DEL can be induced by doping the (001) surface of $SrTiO_3$. As for the interface, the surface 2DEL is confined by a band-bending potential in $SrTiO_3$ and consists of an orbitally polarized ladder of quantum confined Ti t_{2g} electrons that are highly mobile in the surface plane[5–7,14]. Thus far, the surface 2DEL has been studied only at carrier densities around 2×10^{14} cm^{-2}, approximately a factor of five higher than typically observed at the $LaAlO_3/SrTiO_3$ interface[5–7]. In the following, we present ARPES data extending to lower carrier densities that are directly comparable to the $LaAlO_3/SrTiO_3$ interface. We achieve this by preparing $SrTiO_3$(001) wafers *in situ*, which results in well-ordered clean surfaces that can be studied by ARPES over extended timescales, as they are less susceptible to the ultraviolet-induced formation of charged oxygen vacancies reported for cleaved $SrTiO_3$[5,7,15,16]. Details of the sample preparation are given in Methods.

Figure 1a shows an energy–momentum intensity map for a 2DEL with a carrier density of $n_{2D} \approx 2.9 \times 10^{13}$ cm^{-2} estimated from the Luttinger volume of the first light subband and the two equivalent heavy subbands (see Supplementary Section 2). The most striking features of this data are replica bands at higher binding energy following the dispersion of the primary quasiparticle (QP) bands. The replica bands are all separated by approximately 100 meV and progressively lose intensity, but can be visualized up to the third replica in the curvature plot shown in Fig. 1b. From the equal energy spacing of the replica bands we can rule out that they represent distinct subbands arising from quantum confinement[5–7,16]. We thus interpret the replicas as shake-off excitations involving a single non-dispersive bosonic mode coupling electrons of momentum $\mathbf{k}$ and $\mathbf{k}+\mathbf{q}$. From its energy of approximately 100 meV, we can identify this mode as the highest-frequency longitudinal optical phonon branch (LO_4) of $SrTiO_3$[17]. A plasmon mode in the same energy range[17,18] can be excluded on the basis of the negligible density dependence of the mode frequency observed in Fig. 2. Our ARPES data show that the coupling to this mode largely preserves the dispersion in the replica bands, and thus must be restricted to small values of $\mathbf{q}$. This is a hallmark of Fröhlich polarons, quasiparticles formed by an excess electron dressed by a polarization cloud extending over several lattice sites that follows the charge as it propagates through the crystal[2,19–22]. Such a large polaron state preserves band-like transport, but has an increased effective mass m^*. From our ARPES data we can directly quantify this effect. Using a parabolic fit of the band dispersion in Fig. 1a we find $m^*_{xy} \approx 1.4 m_e$. Using a bare band mass of $m_0 = 0.6 m_e$ (refs 7,15) this

[1]Swiss Light Source, Paul Scherrer Institut, CH-5232 Villigen PSI, Switzerland. [2]Department of Quantum Matter Physics, University of Geneva, 24 Quai Ernest-Ansermet, 1211 Geneva 4, Switzerland. [3]Stanford Institute for Materials and Energy Sciences, SLAC National Accelerator Laboratory, Menlo Park, California 94025, USA. [4]Department of Applied Physics, Stanford University, Stanford, California 94305, USA. [5]Institute of Condensed Matter Physics, École Polytechnique Fédérale de Lausanne (EPFL), CH-1015 Lausanne, Switzerland. [6]Helmholtz-Zentrum Berlin für Materialien und Energie, Elektronenspeicherring BESSY-II, 12489 Berlin, Germany. [7]Diamond Light Source, Harwell Campus, Didcot OX11 0DE, UK. [8]SUPA, School of Physics and Astronomy, University of St Andrews, St Andrews, Fife KY16 9SS, UK. [9]School of Physics and NANOTEC-SUT Center of Excellence on Advanced Functional Nanomaterials, Suranaree University of Technology, Nakhon Ratchasima 30000, Thailand. [10]Institute of Applied Physics, Vienna University of Technology, Wiedner Hauptstrasse 8-10/134, A-1040 Vienna, Austria. [11]Laboratory for Solid State Physics, ETH Zürich, CH-8093 Zürich, Switzerland. [12]Geballe Laboratory for Advanced Materials, Stanford University, Stanford, California 94305, USA. [13]SwissFEL, Paul Scherrer Institut, CH-5232 Villigen PSI, Switzerland. *e-mail: zhiming.wang@psi.ch; felix.baumberger@unige.ch

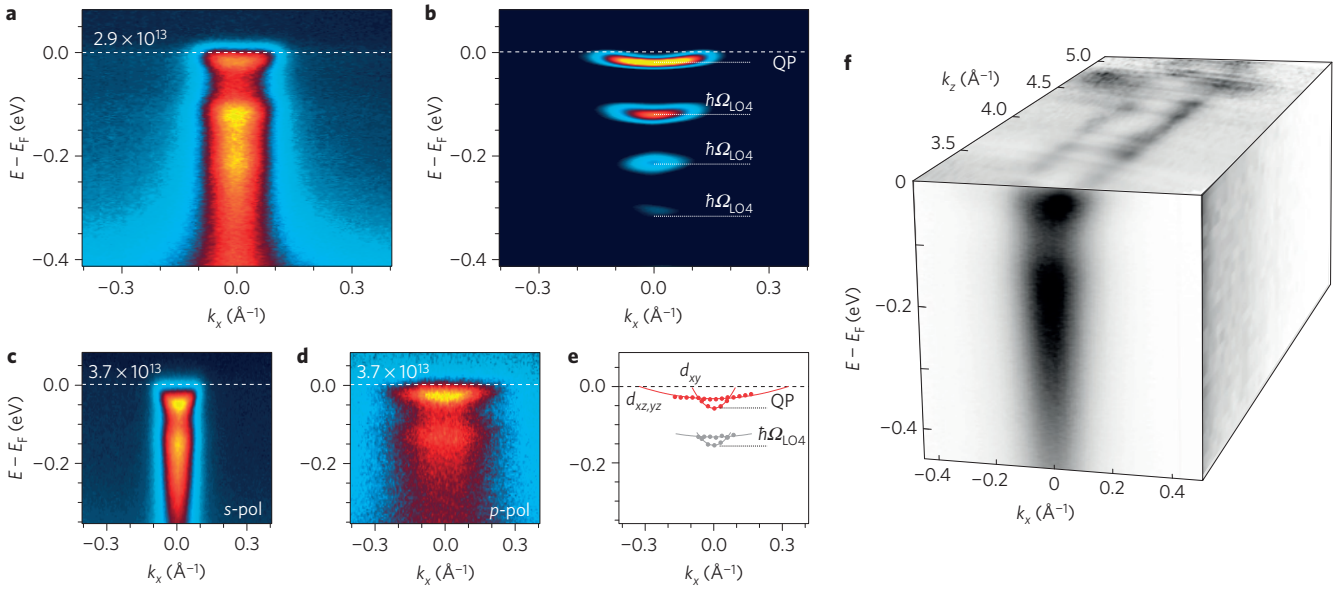

Figure 1 | A two-dimensional liquid of large polarons in $SrTiO_3$. a,b, Energy–momentum intensity map and curvature plot, respectively, for a 2DEL with $n_{2D} = 2.9 \times 10^{13}$ cm^{-2} taken at a photon energy of 44 eV with *s*-polarization (E_F is the Fermi energy and k_x is the crystal momentum along [100]). Note the dispersive replica bands at higher binding energy arising from strong coupling to the LO_4 phonon branch of $SrTiO_3$ with energy $\hbar\Omega_{LO4}$ approximately 100 meV. **c**,**d**, Data taken on a sample with $n_{2D} = 3.7 \times 10^{13}$ cm^{-2} using *s*- and *p*-polarized light, respectively, with a photon energy of $h\nu = 85$ eV to selectively excite the light *xy* and heavy *xz*/*yz* orbitals. **e**, Dispersion of the main and first replica bands extracted from the data in **c** and **d**. **f**, Photon-energy-dependent measurements showing the lack of dispersion along k_z. All data were measured in the second Brillouin zone to avoid the minimum of the matrix elements at normal emission.

corresponds to a mass enhancement $m^*_{xy}/m_0 \approx 2.3$, indicative of an intermediate e–p coupling strength.

In Fig. 1c–f we investigate a sample with slightly higher carrier density. Using *s*- and *p*-polarized light, respectively, we selectively excite electrons from the light *xy* band with approximately 50 meV occupied bandwidth and a shallower heavy band derived from *xz*/*yz* orbitals. Both bands show a clear peak–dip–hump line shape with a dispersive replica band, as summarized in Fig. 1e. This implies that the entire orbitally polarized 2DEL, including the heavy *xz*/*yz* states, which are believed to be important for superconductivity[9–11], is a polaronic liquid at low carrier densities. The lifting of the orbital degeneracy by approximately 20 meV can be attributed to quantum confinement in the band-bending potential which increases the energy of out-of-plane orbitals[7,23]. The reduced dimensionality arising from quantum confinement is visualized directly in Fig. 1f, where we show the absence of dispersion along the surface normal k_z, characteristic of two-dimensional electronic states.

We now turn our attention to the strength of e–p coupling. Its systematic evolution with carrier density in the $SrTiO_3$(001) 2DEL is shown in Fig. 2. Using *s*-polarized light, we resolve a single d_{xy} QP band at low density. Energy distribution curves extracted at k_F show a strongly reduced weight of the coherent QP and at least two phonon satellites, each separated by approximately 100 meV. Empirically, we find that the experimental spectra are described well by a Franck–Condon model using a single phonon mode of approximately 100 meV. Highly restricted fits using the characteristic Poisson distribution $I_n/I_{QP} = a_c^{2n}/n!$ (a_c = constant) for the intensity ratio of the *n*th phonon satellite and the QP peak in the Franck–Condon model are shown in Fig. 2g–l. Details of the fits are described in the Supplementary Information. From this analysis we infer a quasiparticle residue $Z \approx 0.2$ at the lowest density studied here. This is beyond the validity of the perturbation theory result for the Fröhlich model of $Z = 1 - \alpha/2$ (refs 24,25), where α is the dimensionless coupling constant, placing the $SrTiO_3$ 2DEL in a theoretically challenging regime of intermediate coupling. Moreover, the ratio of lattice energy to electron kinetic energy is neither small nor independent of doping, which excludes a Migdal–Eliashberg approach. We therefore estimate α from the experimentally determined quasiparticle residue Z using the results of diagrammatic quantum Monte Carlo simulations of the Fröhlich model reported in ref. 25. This gives $\alpha \approx 2.8$ at the lowest carrier density, comparable to $\alpha = 2$–3 reported for lightly doped bulk $SrTiO_3$ based on an analysis of optical conductivity data[26,27].

As the carrier density increases, the Fermi wavevector increases monotonically, and new subbands become discernible. Concomitantly, the spectral weight of the phonon satellites weakens and, for densities above $n_2 \approx 9 \times 10^{13}$ cm^{-2}, they can no longer be resolved experimentally. At high density, e–p coupling is not only weaker but also of a fundamentally different nature. This is illustrated in Fig. 2f,l. In this regime, the quasiparticle dispersion shows a weak kink at an energy of approximately 30 meV, and no signs of replica bands can be discerned in the raw data or in curvature plots (see Supplementary Fig. 4), providing direct evidence for a suppression of the long-range Fröhlich interaction. Instead, consistent with ref. 7, we find that the spectral function and e–p self-energy of the high-density 2DEL can be described by Migdal–Eliashberg theory with $\lambda \approx 0.7$ and the same coupling to the entire phonon density of states.

To track the crossover from the polaronic state to short-range e–p coupling, we analyse the quasiparticle residue and effective mass of the dispersive bands close to the Fermi level as a function of 2D carrier concentration. The results are summarized in Fig. 3, where we plot m^* obtained from fits to the QP dispersion and $Z(k_F)$ from fits to a Franck–Condon model as described above. Three distinct regimes can be identified. Below $n_1 \approx 4 \times 10^{13}$ cm^{-2}, both quantities depend weakly on carrier density and apparently saturate around $m^* \approx 1.4 m_e$ and $Z(k_F) \approx 0.2$, respectively. At intermediate carrier concentrations of $n_{2D} = 4$–9×10^{13} cm^{-2}, the polaronic state persists, as is seen most directly from the spectra in Fig. 2h–j showing a clear phonon satellite over this entire regime. However, approaching $n_2 \approx 9 \times 10^{13}$ cm^{-2}, where the phonon satellites are no

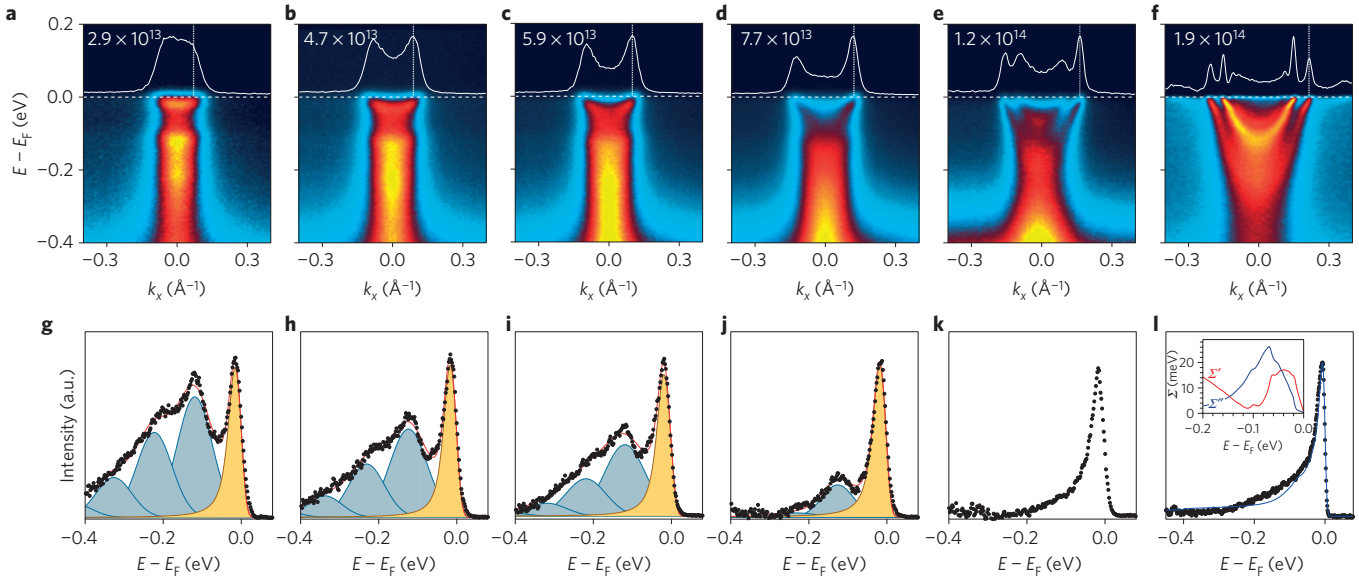

Figure 2 | Evolution of the 2DEL spectral function with carrier concentration. a–f, Raw energy–momentum intensity maps of 2DELs with increasing carrier concentration indicated in units of cm^{-2}. **g–l**, Energy distribution curves (EDCs) at the Fermi wavevector indicated by a vertical dashed white line in the corresponding image plots in **a–f**. An exponential background describing the tail of the in-gap state at approximately −1.1 eV has been subtracted from the raw EDCs (see Supplementary Information). In **g–j** we show fits to a Franck–Condon model with a single phonon mode. The coherent quasiparticle and incoherent phonon satellites are coloured in yellow and blue, respectively. The red line shows the full fit. **l** shows a calculation of the spectral function (blue line) using the conventional Eliashberg e-p self-energy $\Sigma = \Sigma' + i\,\Sigma''$ for the high-density limit found in ref. 7 and reproduced in the inset.

longer resolved experimentally, the quasiparticle residue increases by more than a factor of two to $Z \approx 0.5$, and the effective coupling strength decreases to $\alpha \approx 1.3$. This is opposite to the trend expected for short-range e–p coupling[28], and thus strongly supports our identification of long-range interactions as described by the Fröhlich model. We note that the weak coupling to the LO_4 branch close to n_2 reported in Fig. 3 has recently been confirmed for the $LaAlO_3/SrTiO_3$ interface 2DEL in a soft X-ray ARPES study reporting $Z \approx 0.4$ for a sample with $n_{2D} \approx 8 \times 10^{13}$ cm^{-2}, in excellent agreement with our findings[29].

The effective mass decreases more slowly than the quasiparticle residue, saturating at $m^* \approx 1.0 m_e$ at high density. This slow decrease is characteristic of the Fröhlich model where $Z < m_0/m^*$. For weak to intermediate coupling, the effective mass of Fröhlich polarons can be approximated as $m^*/m_0 = 1/(1-\alpha/6)$ (refs 19,25). As shown in Supplementary Fig. 6, this relation systematically underestimates the effective masses obtained directly from the quasiparticle dispersion, but reproduces their trend as a function of density. We tentatively assign this behaviour to the effect of electron–electron interactions, which is not fully included in the analysis of Z in the polaronic regime. Indeed, the factor between the two effective masses is approximately 1.3, which is consistent with the mass enhancement due to electronic correlations estimated in ref. 7. For densities above n_2, described by Migdal–Eliashberg theory, $Z = m/m^*$, suggesting that the quasiparticle residue saturates around $Z = 0.6$ in the high-density 2DEL.

We attribute the breakdown of the polaronic state at high carrier density to improved electronic screening suppressing the long-range Fröhlich interaction. To estimate the crossover from dielectric screening in the polaronic regime to predominantly electronic screening, we compare the polaron radius $r_p = (\hbar/2m^*\Omega_{LO_4})^{1/2}$ (ref. 19) with the electronic screening length. Using the experimentally determined parameters we find $r_p \approx 6$ Å. Given the relatively large dielectric constant of doped $SrTiO_3$, electronic screening is in the Thomas–Fermi regime and the screening length can be estimated from $r_{TF} = (\epsilon\epsilon_0 E_F/2e^2 n_{3D})^{1/2}$ for a 3D electron liquid (here, ϵ_0 is the permittivity of free space, E_F is the Fermi energy and e is the elementary charge). Assuming a uniform charge distribution n_{3D} over a 2DEL thickness of three unit cells and a static dielectric constant $\epsilon = 100$, which provides a good description of the band-bending potential in the doped surface region[7,16], we

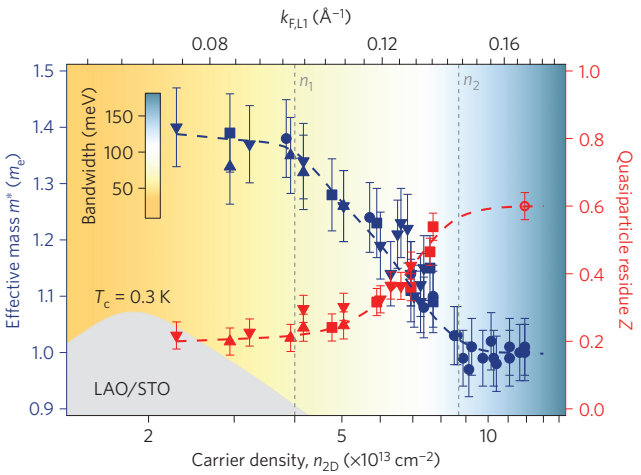

Figure 3 | Effective mass and quasiparticle residue in the $SrTiO_3$ 2DEL. Evolution of the effective mass m^* (blue symbols) and quasiparticle residue Z (red symbols) with carrier density. Different symbols indicate data taken on substrates annealed at different temperatures. Closed red symbols are obtained from Franck–Condon fits, whereas the last value with an open symbol in the adiabatic Migdal–Eliashberg regime has been calculated from $Z = m_0/m^*$. Error bars indicate the reproducibility of our results. An additional systematic error cannot be excluded. The background colour encodes the bare bandwidth of the first light subband calculated from the experimentally determined Fermi wavevector $k_{F,L1}$ of the first light subband shown in the top axis, assuming a bare mass of $m_0 = 0.6 m_e$. Dashed lines are guides to the eye. The dome-shaped superconducting phase with a maximal critical temperature of $T_C = 0.3$ observed at the $LaAlO_3/SrTiO_3$ interface is indicated in grey.

estimate that $r_{TF} = r_p$ for a density $n_{2D} \approx 5 \times 10^{13}$ cm^{-2}, slightly above n_1, where Z starts to increase, progressively resulting in a reduced effective coupling constant α. At higher carrier densities, electronic screening will rapidly become more important, as ϵ decreases simultaneously with the increase in n. We note that the moderate electronic screening length r_{TF} justifies the above use of an expression for 3D electron liquids. This basic picture is consistent with the temperature dependence of the electron mobility in $SrTiO_3$ 2DELs[30], and further confirmed by our calculations of the spectral function reported in Supplementary Fig. 5. Using exact diagonalization of a model Hamiltonian with constant coupling parameter, we find pronounced replica bands at low carrier density, and a rapid suppression of the replicas as the carrier density is increased over the relevant range. These calculations thus reproduce the key experimental findings of our study and support the idea that increasing electronic screening drives the observed breakdown of the polaronic liquid at high carrier densities.

The above results demonstrate that e–p interaction in $SrTiO_3$ based 2DELs is remarkably complex and strongly dependent on carrier density. This provides insight into the superconducting pairing mechanism at the $LaAlO_3/SrTiO_3$ interface, which has so far eluded experimental investigation. As shown in Fig. 3, superconductivity in $LaAlO_3/SrTiO_3$ interface 2DELs[8–10,31] occurs in the polaronic low-density regime, and its suppression on the overdoped side coincides with a gradually decreasing coupling to the LO_4 branch. This supports the notion that superconductivity is phonon mediated[13,32,33] and suggests that the pairing potential is dominated by the exchange of high-frequency longitudinal phonons rather than soft modes. We note that our experimental spectral functions do not exclude the formation of large bipolarons, which have been discussed early on in the context of superconductivity in polar oxides[34,35]. Superconducting susceptibilities calculated within our exact diagonalization scheme reported in Supplementary Section 5 provide additional insight. Although limitations in the Hilbert space size prohibit a quantitative comparison with experiment, the calculations clearly show that the dominant pairing channel has *s*-wave symmetry. Moreover, the saturation of the superconducting susceptibility with carrier density found in this model provides evidence for a competition between the opposite trends of density of states and effective e–p coupling underlying dome-shaped superconductivity in $SrTiO_3$ 2DELs. We note that coupling to the LO_4 branch of $SrTiO_3$ with comparable strength was also invoked to explain the anomalously high superconducting critical temperature of FeSe monolayers on $SrTiO_3$ substrates[2,36].

Methods

Methods and any associated references are available in the online version of the paper.

Received 25 May 2015; accepted 10 March 2016; published online 11 April 2016

References

1. Mannhart, J. & Schlom, D. G. Oxide interfaces—an opportunity for electronics. *Science* **327,** 1607–1611 (2010).
2. Lee, J. J. *et al*. Interfacial mode coupling as the origin of the enhancement of T_c in FeSe films on $SrTiO_3$. *Nature* **515,** 245–248 (2014).
3. Zubko, P., Gariglio, S., Gabay, M., Ghosez, P. & Triscone, J.-M. Interface physics in complex oxide heterostructures. *Annu. Rev. Condens. Matter Phys.* **2,** 141–165 (2011).
4. Ohtomo, A. & Hwang, H. Y. A high-mobility electron gas at the $LaAlO_3/SrTiO_3$ heterointerface. *Nature* **427,** 423–426 (2004).
5. Meevasana, W. *et al*. Creation and control of a two-dimensional electron liquid at the bare $SrTiO_3$ surface. *Nature Mater.* **10,** 114–118 (2011).
6. Santander-Syro, A. F. *et al*. Two-dimensional electron gas with universal subbands at the surface of $SrTiO_3$. *Nature* **469,** 189–193 (2011).
7. King, P. D. C. *et al*. Quasiparticle dynamics and spin-orbital texture of the $SrTiO_3$ two-dimensional electron gas. *Nature Commun.* **5,** 3414 (2014).
8. Thiel, S., Hammerl, G., Schmehl, A., Schneider, C. W. & Mannhart, J. Tunable quasi-two-dimensional electron gases in oxide heterostructures. *Science* **313,** 1942–1945 (2006).
9. Reyren, N. *et al*. Superconducting interfaces between insulating oxides. *Science* **317,** 1196–1199 (2007).
10. Caviglia, A. D. *et al*. Electric field control of the $LaAlO_3/SrTiO_3$ interface ground state. *Nature* **456,** 624–627 (2008).
11. Richter, C. *et al*. Interface superconductor with gap behaviour like a high-temperature superconductor. *Nature* **502,** 528–531 (2008).
12. Cheng, G. *et al*. Electron pairing without superconductivity. *Nature* **521,** 196–199 (2015).
13. Boschker, H., Richter, C., Fillis-Tsirakis, E., Schneider, C. W. & Mannhart, J. Electron–phonon coupling and the superconducting phase diagram of the $LaAlO_3$-$SrTiO_3$ interface. *Sci. Rep.* **5,** 12309 (2015).
14. Plumb, N. C. *et al*. Mixed dimensionality of confined conducting electrons in the surface region of $SrTiO_3$. *Phys. Rev. Lett.* **113,** 086801 (2014).
15. Wang, Z. *et al*. Anisotropic two-dimensional electron gas at $SrTiO_3$(110). *Proc. Natl Acad. Sci. USA* **111,** 3933–3937 (2014).
16. McKeown Walker, S. *et al*. Carrier-density control of the $SrTiO_3$ (001) surface 2D electron gas studied by ARPES. *Adv. Mater.* **27,** 3894–3899 (2015).
17. Gervais, F., Servoin, J.-L., Baratoff, A., Bednorz, J. G. & Binnig, G. Temperature dependence of plasmons in Nb-doped $SrTiO_3$. *Phys. Rev. B* **47,** 8187–8194 (1993).
18. Chang, Y. J., Bostwick, A., Kim, Y. S., Horn, K. & Rotenberg, E. Structure and correlation effects in semiconducting $SrTiO_3$. *Phys. Rev. B* **81,** 235109 (2010).
19. Devreese, J. T. & Alexandrov, A. S. Fröhlich polaron and bipolaron: recent developments. *Rep. Prog. Phys.* **72,** 066501 (2009).
20. Alexandrov, A. S. *Theory of Superconductivity: From Weak to Strong Coupling* (Series in Condensed Matter Physics, Institute of Physics, 2003).
21. Moser, S. *et al*. Tunable polaronic conduction in anatase TiO_2. *Phys. Rev. Lett.* **110,** 196403 (2013).
22. Chen, C., Avila, J., Frantzeskakis, E., Levy, A. & Asensio, M. C. Observation of a two-dimensional liquid of Fröhlich polarons at the bare $SrTiO_3$ surface. *Nature Commun.* **6,** 8585 (2015).
23. Salluzzo, M. *et al*. Orbital reconstruction and the two-dimensional electron gas at the $LaAlO_3/SrTiO_3$ interface. *Phys. Rev. Lett.* **102,** 166804 (2009).
24. Lee, T. D., Low, F. E. & Pines, D. The motion of slow electrons in a polar crystal. *Phys. Rev.* **90,** 297–302 (1953).
25. Mishchenko, A. S., Prokof'ev, N. V., Sakamoto, A. & Svistunov, B. V. Diagrammatic quantum Monte Carlo study of the Fröhlich polaron. *Phys. Rev. B* **62,** 6317–6336 (2000).
26. van Mechelen, J. L. M. *et al*. Electron–phonon interaction and charge carrier mass enhancement in $SrTiO_3$. *Phys. Rev. Lett.* **100,** 226403 (2008).
27. Devreese, J. T., Klimin, S. N., van Mechelen, J. L. M. & van der Marel, D. Many-body large polaron optical conductivity in $SrTi_{1-x}Nb_xO_3$. *Phys. Rev. B* **81,** 125119 (2010).
28. Mishchenko, A. S., Nagaosa, N. & Prokof'ev, N. Diagrammatic Monte Carlo method for many-polaron problems. *Phys. Rev. Lett.* **113,** 166402 (2014).
29. Cancellieri, C. *et al*. Polaronic metal state at the $LaAlO_3/SrTiO_3$ interface. *Nature Commun.* **7,** 10386 (2016).
30. Mikheev, E. *et al*. Limitations to the room temperature mobility of two- and three-dimensional electron liquids in $SrTiO_3$. *Appl. Phys. Lett.* **106,** 062102 (2015).
31. Lin, X. *et al*. Critical doping for the onset of a two-band superconducting ground state in $SrTiO_{3-\delta}$. *Phys. Rev. Lett.* **112,** 207002 (2014).
32. Klimin, S. N., Tempere, J., Devreese, J. T. & van der Marel, D. Interface superconductivity in $LaAlO_3/SrTiO_3$. *Phys. Rev. B* **89,** 184514 (2014).
33. Gorkov, L. P. Phonon mechanism in the most dilute superconductor: n-type $SrTiO_3$. Preprint at http://arxiv.org/abs/1508.00529 (2015).
34. Emin, D. Formation, motion, and high-temperature superconductivity of large bipolarons. *Phys. Rev. Lett.* **62,** 1544–1547 (1989).
35. Hohenadler, M., Aichhorn, M. & Von Der Linden, W. Single-particle spectral function of the Holstein–Hubbard bipolaron. *Phys. Rev. B* **71,** 014302 (2004).
36. Wang, Q.-Y. *et al*. Interface-induced high-temperature superconductivity in single unit-cell FeSe films on $SrTiO_3$. *Chin. Phys. Lett.* **29,** 037402 (2012).

Acknowledgements

We thank A. Fête, M. Grilli, L. Patthey, V. Strocov, J.-M. Triscone, D. van der Marel and Z. Zhong for discussions. The ARPES work was supported by the Swiss National Science Foundation (200021-146995). The spectral function calculations were supported at SLAC and Stanford University by the US Department of Energy, Office of Basic Energy Sciences, Division of Materials Sciences and Engineering, under Contract No. DE-AC02-76SF00515, and by the Computational Materials and Chemical Sciences Network (CMCSN), under Contract No. DE-SC0007091. A portion of the computational work was performed using the resources of the National Energy Research Scientific

Computing Center supported by the US Department of Energy, Office of Science, under Contract No. DE-AC02-05CH11231. M.S. acknowledges financial support by the Sino-Swiss Science and Technology Cooperation (No. IZLCZ2138954), J.S.-B. by the Impuls- und Vernetzungsfonds der Helmholtz Gemeinschaft (Grant No. HRJRG-408), P.D.C.K. by the UK-EPSRC (EP/I031014/1) and the Royal Society, U.D. by the ERC Advanced Grant 'OxideSurfaces' and W.M. by the Thailand Research Fund (TRF) under the TRF Senior Research Scholar, Grant No. RTA5680008. We acknowledge Diamond Light Source for time on beamline I05 under proposal SI11741.

Author contributions

ARPES measurements were carried out by Z.W., S.M.W., Z.R., F.Y.B., A.d.l.T., S.R., M.R. and F.B. and analysed by Z.W., A.T. and F.B.; N.C.P., M.S., P.H., J.S.-B., A.V., T.K.K. and M.H. were responsible for the synchrotron beam lines used in the experiments; Y.W., B.M. and T.P.D. performed the exact diagonalization calculations. F.B. wrote the manuscript with contributions by Z.W., Y.W. and A.T.; T.P.D., M.R. and F.B. were responsible for project planning, direction and resources. All authors contributed to the scientific discussion of the results.

Additional information

Supplementary information is available in the online version of the paper. Reprints and permissions information is available online at www.nature.com/reprints. Correspondence and requests for materials should be addressed to Z.W. or F.B.

Competing financial interests

The authors declare no competing financial interests.

Methods

The Nb-doped (0.5 wt%) and La-doped (0.075 wt%) $SrTiO_3$(001) surfaces were prepared by mild Ar^+ sputtering (600 eV, 2 μA, 5 min) followed by annealing in 2×10^{-6} mbar oxygen for 0.5 h at temperatures varying from 700 to 1,000 °C, as monitored by an infrared pyrometer. Consistent with measurements on *in-situ*-prepared and cleaved $SrTiO_3$, we find no spectral weight in the entire bulk bandgap on freshly prepared surfaces (see Supplementary Fig. 1)[5,15,16]. Quantum confined metallic states are apparently concomitant with a localized in-gap state at higher energy after exposure of the surface to synchrotron light[5,15,16]. We find that the rate at which the 2DEL carrier density increases under the synchrotron beam increases with the annealing temperature, then exploit this to stabilize low carrier densities over the extended exposure times required for detailed ARPES measurements. ARPES measurements were performed at the SIS beamline of the Swiss Light Source, the I05 beamline of Diamond Light Source and the 1^2 beamline of BESSY II at the Helmholtz-Zentrum Berlin. Data were acquired at $T \approx 20$ K with $h\nu = 30$–100 eV and energy and angular resolutions of 10–25 meV and ∼0.2°, respectively.